Positron annihilation spectroscopy investigation of vacancy defects in neutron-irradiated 3C-SiC

Xunxiang Hu, Takaaki Koyanagi, Yutai Katoh, and Brian D. Wirth

Phys. Rev. B **95**, 104103 — Published 10 March 2017

DOI: 10.1103/PhysRevB.95.104103

Positron Annihilation Spectroscopy Investigation of Vacancy Defects in Neutron-Irradiated 3C-SiC ¶

Xunxiang Hu [1], Takaaki Koyanagi [1], Yutai Katoh [1], Brian D. Wirth [1, 2]

[1] Oak Ridge National Laboratory, Oak Ridge, TN 37831 USA

[2] University of Tennessee, Knoxville, TN 37996 USA

Abstract:

Positron annihilation spectroscopy characterization results for neutron-irradiated 3C-SiC are described here, with a specific focus on explaining the size and character of vacancy clusters as a complement to the current understanding of the neutron irradiation response of 3C-SiC. Positron annihilation lifetime spectroscopy was used to capture the irradiation temperature and dose dependence of vacancy defects in 3C-SiC following neutron irradiation from 0.01 to 31 dpa in the temperature range from 380 to 790°C. The neutral and negatively charged vacancy clusters were identified and quantified. The results suggest that the vacancy defects that were measured by positron annihilation spectroscopy technique contribute very little to the transient swelling of SiC. In addition, coincidence Doppler broadening measurement was used to investigate the chemical identity surrounding the positron trapping sites. It was found that silicon vacancy–related defects dominate in the studied materials and the production of the antisite defect C_{Si} may result in an increase in the probability of positron annihilation with silicon core electrons.

1. Introduction

Silicon carbide (SiC) has been considered for use in nuclear systems as a fuel and structural material since the 1960s, because of its high-temperature strength, chemical inertness, and exceptional irradiation resistance [1]. Chemically vapor deposited (CVD) SiC has been used as a pressure vessel material for the tristructural-isotropic fuel particles for high temperature gas-cooled reactors and novel accident tolerant fuel concepts for light water reactors [2]. The use of SiC/SiC composites as the structural materials has also been proposed in various advanced fission reactor concepts and fusion reactors [3] [4]. Driven by the need to increase the safety margins of nuclear reactors in accident scenarios, the research and development of accident-tolerant fuel has become important in the nuclear engineering and materials community. A continuous fiber SiC/SiC composite cladding is under consideration as a possible replacement for zirconium alloy cladding [5]. The extremely hostile environments in fission and fusion reactors—characterized by intense neutron radiation, high temperature, aggressive corrosive

coolants, high thermal flux, high particle flux and other features—impose significant challenges to SiC by altering its microstructure and physical properties.

Microstructural development and physical-mechanical property changes in SiC subjected to neutron and ion irradiation have been studied extensively [1,3,6-8]. Katoh et al. [8] summarized the irradiation temperature and dose dependence of the microstructures of neutron- and ion- irradiated cubic SiC based on transmission electron microscope (TEM) observations. At relatively low temperatures (<~800°C), irradiation-produced defect features visible in TEM were small dislocation loops and black dots, which at high temperatures (>~1000°C) collapsed into Frank faulted loops at intermediate fluence and finally developed into a dislocation network at very high fluences. Cavities were observed by TEM only at irradiation temperatures higher than ~1000°C. The irradiation effects upon SiC subjected to high-energy particle irradiation included thermal and electrical transport property changes and dimensional change, or swelling [1,8,9]. In particular, the transient swelling, which exhibits a strong dependence on the irradiation temperature below ~1000°C, is considered a critical phenomenon that dictates secondary stresses in irradiated SiC in the presence of an irradiation temperature gradient within the material. Transient swelling in SiC is known to arise from the accumulation of point defects and/or clusters that are not examined or quantified in the conventional electron microscopy. Therefore, the contribution of various kinds of defects to the transient swelling in SiC is only insufficiently understood and the characterization of the TEM-invisible defects in SiC remains an open question.

Properties of intrinsic defects (vacancies, interstitials, and antisites) in SiC have previously been studied with various techniques. Electron paramagnetic resonance (EPR) spectroscopy [10] [11] [12] has been used to study silicon (Si) and carbon (C) vacancies in SiC based on the observation of the hyperfine interaction with ^{29}Si (nuclear spin I=1/2, natural abundance of 4.7%) and ^{13}C (I=1/2, 1.1%) nuclei. In addition, photoluminescence [13], deep level transient spectroscopy [14], and magic angle spinning nuclear magnetic resonance spectroscopy (an element specific technique) [15] have also been used to characterize the defects in irradiated SiC. However, information on the sizes and concentrations of vacancy clusters in SiC cannot be determined from these techniques. In contrast, positron annihilation spectroscopy (PAS) is a well-established tool for investigating open-volume defects in condensed materials [16], and has been extensively employed to characterize the vacancy-type defects in as-grown [17,18] [19] or irradiated SiC [20-23] [19,24-26]. Positron annihilation lifetime spectroscopy (PALS) is most commonly used to identify the sizes and concentrations of the vacancy clusters present within the materials. However, most of the available PAS studies of SiC have been focused on high-energy electron- or proton-irradiated SiC. The available PAS data for neutron-irradiated SiC are very limited. Xu et al. [27] applied PALS measurements and coincidence Doppler broadening (CDB) to investigate the evolution of vacancy-type defects in neutron-irradiated single crystalline 4H-SiC ($3.2\times10^{21}m^{-2}$, E>1MeV, at 20°C) during isochronal annealing to define the recovery stages. PALS measurements were also used by Akiyoshi et al. [20] to study the correlation between vacancy-type defects and the thermal diffusivity in fast neutron-irradiated 3C-SiC manufactured by hot press sintering. The results indicated no significant change in the mean positron lifetime in these heavily

neutron-irradiated (28~42 dpa) specimens at irradiation temperatures of 500~738°C. However, the identification and quantification of the detected vacancy clusters present in the studied SiC samples are lacking. The results based on the SiC samples used in these studies [20] [27] provide very limited insights into understanding neutron irradiation response of the high purity CVD 3C-SiC, the leading SiC for nuclear applications. Therefore, systematic PAS characterization of neutron-irradiated, high-purity 3C-SiC is needed to provide a more complete picture of the evolution of small, TEM-invisible vacancy clusters, because such clusters are suspected to play a role in the swelling, radiation creep, and thermal conductivity degradation of neutron-irradiated SiC [1]. Moreover, the application of the CDB technique would enable the determination of the chemical identities surrounding positron trapping sites. Yet, CDB measurements have not been widely used in previous positron studies of irradiated SiC.

In the present study, PALS measurements were performed to characterize the vacancy-type defects in 3C-SiC exposed to various neutron irradiation conditions, and to evaluate their dependence on temperature and irradiation dose. CDB measurements were performed to identify the chemical signatures of the positron trapping sites. The roles of the detected vacancy defects in the transient swelling regime of neutron-irradiated 3C-SiC are discussed. This new information on vacancy cluster evolution following neutron irradiation complements and extends the current understanding of the neutron irradiation response, in particular, the contribution of vacancy clusters to irradiation induced swelling of 3C-SiC in the transient swelling regime.

2. Experiments

2.1. Materials and neutron irradiation

High purity (>99.9995%) polycrystalline 3C-SiC monolithic samples were used in this study. The samples were synthesized by Rohm and Hass Co. (now Dow Chemical Co.) by the CVD process. Neuron irradiation was performed in the flux trap position of the High Flux Isotope Reactor (HFIR) at Oak Ridge National Laboratory (ORNL) within aluminum capsules that contained a molybdenum container to hold the specimens. The capsules were filled with high-purity helium and were irradiated under a fast neutron flux of 1×10^{19} n/m^2/s (E > 0.1 MeV) corresponding to a damage rate of $\sim1\times10^{-6}$ dpa (displacement per atom)/s in SiC [28]. Therefore, 1 dpa is equivalent to an exposure to a fast neutron fluence of 1×10^{25} n/m^2. The irradiation conditions of the 3C-SiC studied are summarized in Table 1.

2.2 Positron annihilation spectroscopy

Following neutron exposure in HFIR, the samples were removed from the capsules and cleaned in alcohol using an ultrasonic cleaner. Two identical 5×5×1mm disks were sectioned from the original sample by using a low-speed diamond saw. The samples used for PAS measurements had a conventional sample-source-sample geometry and were prepared by directly evaporating a 20μL $Na^{22}Cl$ solution (~3.7×10^5 Bq) onto the surface of one of the two disks and, after the water evaporated, then covering that disk with the other disk. This "sandwich" was then wrapped in 10μm thick aluminum foil. PAS measurements were performed at room temperature using the PAS system established within the Low-Activation Materials Development and Analysis lab at ORNL [29]. The system simultaneously measures the time and energy of the two annihilation gamma rays to enable both PALS and CDB analysis. The PALS measurement operates in a double-stop mode and has a calculated system time resolution of ~160 ps. Each recorded lifetime spectrum contained a total of ~2×10^6 counts and was analyzed by fitting the exponential decay of two lifetime components, after deconvolution of the experimental resolution function, which we approximated as a weighted sum of three Gaussians. Data analysis was performed using PALSfit3 developed by Technical University of Denmark [30]. The energies of the two annihilation gamma rays used for CDB analysis were measured by two HPGe detectors facing the sample-source-sample sandwich from opposite sides. 1×10^7 annihilation events were collected for the Doppler-broadening spectra. The experimental setup for CDB measurement had a data/background ratio of 5×10^4. More details for this PAS system are provided in Ref. [29].

3. Results and discussions

3.1 Positron annihilation lifetime spectroscopy

3.1.1 Qualitative analysis of PALS

In order to illustrate directly the influence of neutron irradiation on the measured positron lifetime, Fig. 1 plots the normalized positron lifetime spectra (assuming the peak counts to be unity at zero time) of 3C-SiC irradiated at three different temperature ranges —(a) 380~440°C, (b) 500~540°C, and (c) 750~790°C—to capture the irradiation dose dependence. These data are plotted separately for the sake of clarity. An apparent increase in the long lifetime portions of the spectra of all irradiated samples was observed in comparison with that of the reference SiC sample. For the samples irradiated in the same temperature range, the long lifetime parts of the measured spectra became more intense with increasing radiation dose. The highest irradiation dose (~30 dpa) promoted the most significant enhancement of the long lifetime components. The increase in the long-positron lifetime component of the spectra indicates an increase in either the concentrations or the sizes of the vacancy-type defects present within the studied SiC samples with increasing neutron exposure.

Fig. 2 shows the influence of irradiation temperature on the normalized positron lifetime spectra at two irradiation doses, i.e., (a) 0.11 dpa and (b) ~30 dpa, respectively. Owing to the extremely high migration energies of Si (2.4 eV) and C (3.5 eV) vacancies in SiC [31,32], they are believed to be effectively immobile in the two lower irradiation temperature ranges; whereas mobility of Si vacancy is expected at the higher irradiation temperatures from 750 to 790°C, although to a very limited extent. The neutron dose shown in Fig. 2 (a) is only 0.11 dpa, resulting in insignificant defect evolution. Thus, it is not surprising that the observed lifetime spectra are similar across all three irradiation temperatures. In contrast, Fig. 2 (b) shows that the positron lifetime spectrum of TTN07 irradiated to 29 dpa at 750°C has a clearly increased long-lifetime component compared with the results of the lower temperature irradiations. This spectrum shift indicates the formation of larger vacancy clusters with longer positron lifetimes as a result of Si vacancy migration. In addition, no significant changes in the lifetime spectra of the two samples, TTN03 and TTN05, irradiated at 440 and 500°C, respectively, were observed. That finding is consistent with the assumption of very limited to nonexistent vacancy mobility in 3C-SiC below about 750°C.

3.1.2 Quantitative analysis of PALS

Fitting the measured positron lifetime spectra with two components using PALSfit3 provided a sufficient fit to the experimental data. We also evaluated the use of three- or four-component fitting, but these did not reproduce the measured lifetime spectra sufficiently or the fitting values of the parameters are unphysical. Correspondingly, in the present study, the measured PALS spectra of all samples were decomposed into two lifetime components by first subtracting the background. The decomposition generated parameters for further analysis, such as positron lifetimes described as τ_1, short lifetime; τ_2, long lifetime; and I_i, the associated intensity of each component. The average positron lifetime $< \tau >$ is simply the geometric mean calculated from $< \tau >= \tau_1 I_1 + \tau_2 I_2$, where $I_1+I_2=1$. In contrast to PAS measurements using a sealed positron source, the source component resulting from positron annihilation in a source wrapping foil (e.g., thin Kapton or Mylar films, Ti or Al foil) was neglected and is not resolved in the present study, because the $Na^{22}Cl$ solution was directly deposited onto the sample surface (<1% source term). The evolution of the lifetime components as a function of irradiation dose and temperature is plotted in Fig. 3. Under neutron irradiation, defect creation in displacement cascades produces a more complex damaged microstructure. The presence of detectable vacancy clusters in neutron-irradiated 3C-SiC is correlated to the increase in the measured positron lifetimes, as shown in Fig. 3. The general observation is that higher radiation dose promotes an increase in the long lifetime (τ_2) component, indicating the growth of vacancy-type defects. The intensity of this long lifetime component in the neutron-irradiated samples was quite large under all conditions, with values greater than 90%. The mean lifetime ($<\tau>$) also increased with increasing neutron exposure for the samples irradiated in each temperature range, as shown in Table 2.

The measured short lifetimes (τ_1) varied over a range of 15~73 ps; they are less than the bulk lifetime, since $\tau_1=1/(\tau_B^{-1}+\kappa)$, where τ_B is the bulk lifetime (140 ps for SiC) and κ is the positron trapping rate. The derivation of this expression will be discussed further in

Section 3.1.3. Here we would like to emphasize that the correlation between τ_1 and κ can be used to validate the self-consistency of the two-state trapping model. The τ_1 predicted by using the fitting parameters is shown in the bottom plot of Fig. 3 in the form of black hollow symbols; it is in good agreement with the experimentally obtained τ_1.

The long positron lifetimes of these samples, resulting from positron trapping in the vacancy-type defects, are listed in Table 2. Table 2 also identifies the possible nature of the detected vacancy clusters. Of course, the nature of defects in SiC is complicated by the possibility of various charge states; and correspondingly, the defect charge determines whether or not it could efficiently be detected by PAS. Positively charged vacancy defects will have the lowest probability for positron annihilation as a result of the long-range, repulsive Coulomb interaction between the positive charge and the positron. According to theoretical calculations [33] and EPR measurements [34], the C vacancy in SiC is positively charged. Therefore, C vacancies and positively charged vacancy complexes such as V_C-rich vacancy clusters in SiC are much less likely to trap positrons than is a neutral or negatively charged vacancy or vacancy clusters.

The bulk lifetime value of 3C-SiC has been reported to be 140 ± 4 ps [21,35] . In the present study, the measured positron lifetime spectrum of the as-received polycrystalline 3C-SiC was also resolved into two lifetime components, for which the mean lifetime of 165 ps was greater than the theoretical value of the positron lifetime in perfect SiC. The long lifetime of 196 ± 1 ps indicates the existence of vacancy-type defects. The identification of the detected defects is often carried out based on a comparison between the measured and the theoretical positron lifetime values of known defects. The calculated positron lifetime of a neutral Si vacancy in 3C-SiC ranges from 190 to 210 ps [21]. The Si vacancy is relatively stable over a large range of electron chemical potential when in negative charge states [36]. The positron lifetimes of negatively charged vacancies are expected to be shorter than those of the neutral vacancies. This is because the additional negative charge(s) will increase the positron annihilation rate, as well as influence the localization and relaxation processes of the positron trapping. However, Wiktor et al. [36] report that the differences between the lifetimes of neutral and negatively charged defects are relatively small, ~ 5 ps. Therefore, the positron lifetime of a negative Si vacancy in 3C-SiC is likely in the same range as that of a neutral Si vacancy. In addition, an Si vacancy is a metastable defect that transforms into a C vacancy-antisite complex (V_C-C_{Si}), as widely reported in the literature [31,37,38]. The theoretical positron lifetime of this complex is determined as 197 ps. In spite of its metastability, Si vacancy should still be detected in this case since the associated transformation is a process that is activated only at higher temperatures to overcome the energy barrier of 1.3 eV [37]. Therefore, we deduce that the preexisting defect in the as-received sample was in the form of V_{Si}. Actually, native vacancies or vacancy clusters are often detected in high-purity SiC. Aavikko et al. [18] reported that the as-grown high-temperature CVD 4H-SiC contained vacancy clusters consisting of four or five missing atoms and negatively charged, Si-vacancy-related defects with a measured long lifetime component of 250 ps. Similarly, Ling et al. [17] attributed the measured long lifetime component of 200±9 ps, to the presence of V_{Si}-related defect in as-grown 6H-SiC.

The identification of specific vacancy clusters in materials by using PAS is always difficult owing to the requirement for accurate theoretical predictions of positron lifetimes for all possible vacancy defects contained in the studied materials. As well, positron lifetimes can be very similar for different defects in some cases. In the current study of neutron-irradiated 3C-SiC, the various charge states and configurations of the detected defects further complicated the interpretation of the measured long lifetime.

Here, we attempt to list the vacancy defects that have similar positron lifetime values in comparison with the measured long lifetimes based on available theoretical calculations, thus, providing insights into the defect types possibly present within the irradiated samples. For the two samples irradiated to 0.01 dpa, T8A1 and T8B1, the similar long lifetime gives rise to the possible identification of a $V_{Si} + V_C$ di-vacancy, which is found to be neutral for a wide range of electron chemical potential [35]. For T8D1, irradiated at a higher temperature, 790°C, a much longer lifetime was obtained, which is consistent with a neutral $(V_{Si} + V_C)_2$ tetra-vacancy cluster. The formation of this larger vacancy cluster defect is also consistent with the idea that the thermal diffusion of Si vacancies, and corresponding clustering, does occur at 790°C in 3C-SiC. Further, since this cluster is a stoichiometric defect, this tetra-vacancy is believed to be neutral in 3C-SiC because of its neutral charge stability [35]. Although the stabilities of all $(V_{Si} + V_C)_n$ type defects are not examined in Ref. [35], it is most likely that this type of stoichiometric defect has a neutral charge stability. For the other two samples irradiated to ~0.11 dpa, T8A2 and T8B2, the long lifetime positron annihilation center was identified as $2V_C + V_{Si}$, which is most likely neutral in 3C-SiC to be detected. The defect identified as the long lifetime defect in specimen TTN01 (380°C, 1.5 dpa) is also a $2V_C + V_{Si}$ tri-vacancy.

As well, we identify a neutral $(V_{Si} + V_C)_2$ tetra-vacancy as the dominant vacancy cluster in specimen TTN03, irradiated to a relatively high dose of 31 dpa at 440°C. The thermal diffusion of Si and C vacancies in 3C-SiC should be negligible at this low temperature, and thus we posit that a combination of radiation-enhanced diffusion along with cascade overlap may be responsible for the formation of this tetra-vacancy cluster. Notably, a somewhat larger vacancy cluster of $3V_{Si} + 2V_C$ is identified as the dominant long positron lifetime trapping feature in the specimen TTN05 irradiated to 29 dpa at the slightly higher temperature of 500°C. The long lifetime component of this sample was measured to be 275 ps, which is between the positron lifetime values for $(V_{Si} + V_C)_2$ and $(V_{Si} + V_C)_3$. Therefore, the existing defect is expected to be larger than $(V_{Si} + V_C)_2$ and smaller than $(V_{Si} + V_C)_3$. Thus, it is plausible to expect it to consist of either $3V_{Si} + 2V_C$ or $2V_{Si} + 3V_C$. Since the addition of one C vacancy to a vacancy cluster is observed to have a negligible impact on the calculated positron lifetime [35] , we concluded that $3V_{Si} + 2V_C$ was more likely in this case. Further, this particular vacancy cluster should be a stable defect and have a negative charge. Specimens, T8E1 and TTN07, irradiated at 760 and 750°C to 1.4 dpa and 29 dpa, respectively, contained defects that we identified as $(V_{Si} + V_C)_3$ and $(V_{Si} + V_C)_4$, respectively.

It is commonly accepted that C vacancy has very high migration energy, ~3.5 eV, and is considered immobile in the studied temperature range. In addition to the C vacancy clustering arising from radiation-enhanced diffusion and the severe displacement cascade

overlap, the transformation of metastable V_{Si} to a V_C-C_{Si} complex at these irradiation temperatures may also play a role. Moreover, it is noted that the measured long lifetime is a superposition of the lifetimes of positrons trapped in all the defects present within the materials. Therefore, the examples of the possible defect clusters listed in Table 2 should really be considered to be "average" defect sizes.

It is known that the positron lifetime increases with increasing defect size and eventually saturates toward the lifetime associated with positronium formation near a free surface of 479 ps [39]. The maximum long lifetime acquired from fitting the measured positron lifetime spectra is 294 ps in the case of TTN07, which sets the largest vacancy cluster size investigated in this study. However, this value is still much smaller than that of the saturated lifetime for large vacancy clusters. Therefore, the present analysis excludes the possibility of the significant formation of large vacancy clusters in the 3C-SiC irradiated up to 31 dpa at temperatures lower than 790°C. This result is consistent with the MD simulation of displacement cascades in SiC [40], showing that the cascade lifetime in SiC is very short, about 10 times shorter than that in metals and alloys, and the surviving defects are dominated by Frenkel pairs. The small displacement cascade and the immobile nature of the produced vacancies in the studied temperature range, except the limited mobility of the Si vacancy at the highest irradiation temperature, inhibit the growth of large vacancy clusters.

3.1.3 Determination of defect concentration

The vacancy defect concentration can be estimated in the framework of the two-state trapping model, in which positrons are assumed to annihilate with electrons in the bulk state or in the trapped state in vacancy-type defects [41]. The positron lifetimes obtained by fitting the measured lifetime spectra are expressed as:

$$\tau_1 = \frac{1}{\tau_B^{-1} + \kappa} \tag{1}$$

$$\tau_2 = \tau_V \tag{2}$$

where τ_B is the positron lifetime in the bulk, which is 140 ps in 3C-SiC; τ_V is the positron lifetime in vacancy-type defects; and κ is the net positron trapping rate of the defects:

$$\kappa = \frac{I_2}{I_1}(\tau_B^{-1} - \tau_2^{-1}) \tag{3}$$

The trapping rate is usually assumed to be proportional to the defect concentration (C_V),

$$\kappa = \mu C_V \tag{4}$$

where μ is the specific positron trapping coefficient for each defect, and is a function of defect type, charge state, and size.

The specific positron trapping coefficients for vacancies at 300K typically range between 0.5×10^{15} and 5×10^{15} s^{-1} in semiconductors. The values of this parameter for the neutral and negative defects have been found to differ by about a factor of 1.5~3.5. In this work, we use a factor of 2. Therefore, for a trapping coefficient of a neutral Si vacancy of 0.55×10^{15} s^{-1}, a value of 1.1×10^{15} s^{-1} is expected for the negative Si vacancy, as reported in Ref. [24]. For small neutral vacancy clusters, Brauer et al. [21] assumed that $\mu_{V_n} = n\mu_V$ for a cluster of n vacancies. However, the positron trapping rate into defects is determined by two processes, i.e., first the diffusion of the positron to the trap and secondly the transition into the trap. Considering that the positron diffusion is sufficiently fast, the trapping ability of a defect is limited by the transition rate, which is proportional to the surface area of the defect, or r^2, where r is the equivalent trapping radius of a defect [41]. Therefore, we assume that $\mu_{V_n} = \frac{r_{V_n}^2}{r_V^2}\mu_V$, where r_{V_n} is the equivalent radius of a cluster containing n vacancies. The specific trapping coefficients used in this study are listed in Table 3. Substituting the fitted parameters (shown in Fig. 3) into Eqs. (1-4), together with the application of the corresponding specific trapping coefficients, results in the prediction of the number density of the detected vacancy-type defects in neutron-irradiated 3C-SiC. The results are shown in Table 3. Note that determining the positron coefficient is not an easy task and the uncertainty of μ for a specific defect is roughly a factor of 2~3, which also linearly changes the predicted defect concentration. Thus, large uncertainties are expected for the predicted number density.

3.1.4 Swelling contribution from PAS-detectable vacancy defects in SiC

The neutron damaged microstructure of SiC produces swelling that accompanies a thermal conductivity decrease. One well-known phenomenon in SiC in the irradiation temperature regime investigated here is the transient swelling, which is known to be inversely proportional to temperature and to saturate with increasing dose. For irradiation temperatures above the amorphization threshold (~150°C) and below the transition to the void swelling regime (>~1000°C), the swelling of SiC increases following a power law with dose until it approaches saturation, with a steady decrease in the saturation swelling level with increasing irradiation temperature [9,42]. This temperature range from 150~1000°C is referred to as the "transient swelling" regime, in which only C and Si interstitials are sufficiently thermally mobile in SiC. Therefore, it is supposed that the swelling of SiC in this regime is caused by the accumulation of matrix defects such as isolated vacancies, self-interstitial atom clusters, and anti-site defects, while the contribution of vacancy type-defects to the observed swelling remains a matter of debate.

In Section 3.1.3, the number densities of the possible PAS-detectable vacancy clusters were determined. Correspondingly, we can calculate the contribution of these vacancy clusters to the volumetric swelling of SiC by simply assuming that the atomic volume of these vacancy clusters is equivalent to the volume swelling of the sample without considering the relaxation volumes. Fig. 4 shows a comparison of the measured swelling data and the calculated volume swelling based on the PAS lifetime analysis. In general, the volume swelling derived from PAS data was about two orders of magnitude lower than the measured values. The measured swelling data showed a clear negative

dependence on irradiation temperature. However, this was not observed in the prediction based on the PAS lifetime analysis. Therefore, our results indicate that the swelling contribution of neutral or negatively charged vacancy-type defects in neutron-irradiated SiC as measured by PAS is very minor. Note that PAS may be sensitive to only a fraction of the existing vacancy defects in the neutron-irradiated SiC, i.e., the neutral and negatively charged vacancy defects. MD simulations of the displacement cascade in SiC [40] did reveal that more C defects survive, and these most likely are positively charged. Furthermore, the transformation of Si vacancy to V_C-C_{Si} complex can also reduce the Si vacancy concentration. Further work is needed to elucidate the underlying mechanisms controlling the swelling of SiC exposed to neutron irradiation, but these results certainly indicate very little contribution of vacancy clusters to the transient swelling of SiC subjected to neutron irradiation.

Moreover, the concentration of missing Si atoms from the original lattice sites could be determined based on the PAS-detected vacancy clusters. These displaced Si atoms exist either in the interstitial sites or in the form of antisite defects, which contribute to the transient swelling as well. However, due to the fact that the individual swelling contribution of interstitial and antisite defects of SiC are still an open question and the detailed distribution of these missing Si atoms is unknown, the swelling contribution from these Si atoms will not be discussed in the current study.

3.2 Coincident Doppler Broadening

Positrons eventually are annihilated by electrons, and this annihilation predominantly produces two gamma rays travelling in approximately opposite directions, as is necessitated by energy and momentum conservation during annihilation. The total energy of the two annihilating gamma rays is Doppler shifted as a result of sharing the net center of mass momentum of the positron-electron pair. Thus, in the annihilation process, one gamma ray is upshifted in energy, while the other is downshifted. The energy shift of each photon is expressed by

$$\Delta E = \frac{1}{2} p_L c = \frac{1}{2} \theta_L m_0 c^2 \tag{5}$$

where ΔE is the photon energy difference from the nominal value (511keV), p_L is the corresponding longitudinal momentum shift along the direction of gamma ray emission, in an atomic unit (1 a.u.=7.28 mrad × $m_0 c$), and θ_L is the angular deviation of the photons from 180°. Since p_L has element-specific spectral distributions that correspond to the momentum distributions of the annihilation electrons, analysis of the orbital electron momentum spectrum (OEMS) provides information on the local chemical environment where the positron annihilates. The OEMS is typically represented as the fraction of annihilation events at each momentum interval as a function of p_L, normalized by the measured spectrum of a reference SiC sample (so-called ratio curves).

Fig. 5 shows the ratio curves of the normalized OEMS, in which the momentum spectra of the annihilation photons measured from neutron-irradiated samples have been divided by those of un-irradiated 3C-SiC. As expected, after irradiation, the ratio curves were higher than 1 in the low momentum region (p_L <~ 0.4 a.u.), since positrons have a high possibility of being annihilated with the valence electrons of atoms around a vacancy-type defect in irradiated 3C-SiC. In turn, the high momentum region, which results from positron annihilation with core electrons, was reduced. In addition, the contributions from the positron annihilation events occurring in SiC bulk matrix were limited and could be neglected, given that the longer lifetime intensities of the neutron irradiated samples were greater than 90%. For the samples irradiated in the two lower temperature ranges, as shown in Figs. 5 (a) and (b), the low momentum parts were enhanced and the intensities of the high momentum parts were decreasing with increasing radiation dose. However, the change in the ratio curves of the samples irradiated to dose levels greater than 0.11 dpa was insignificant, implying similar damaged microstructures in these samples in general, and relatively little change with increasing dose. The irradiation dose dependence was more significant for 3C-SiC irradiated at 750~790°C, as shown in Fig. 5 (c). The high temperature did promote the formation of larger vacancy clusters, which agreed with the positron lifetime analysis. In order to elucidate the damage production under various irradiation conditions, the CDB spectra of 3C-SiC were compared with those of unirradiated C and Si. The Si peak appeared in the high momentum region at ~ 2.6 a.u., whereas C peaked at ~ 1.4 a.u., as shown in Fig. 6. For the samples irradiated to 0.01 dpa (T8A1 and T8B1), the ratio curves showed a prominent C peak in the high momentum region; this result indicated that the positrons were mainly trapped at Si related vacancy defects surrounded by C, since the electron momentum in the higher momentum region arose from the positron annihilation with core electrons of C around Si vacancies. In contrast, the Si peak is much weaker because positively charged C vacancies surrounded by Si atoms have a lower probability of trapping positrons. The Si peak signals mainly arose from the positron annihilation events with the core electrons of Si atoms surrounding $(V_{Si}+V_C)_n$. Because of the much higher positron affinity of C [43], positrons have a higher probability of being annihilated with core electrons of C in comparison with that of Si, although the annihilations with valence electrons are still prominent. Therefore, the electron momentum spectra associated with the Si peak were always at a low level. For all other samples irradiated to dose levels greater than 0.1 dpa, the prominent C peak disappeared. However, the insignificant variations in the high momentum regions at all irradiation conditions restricted the qualitative analysis to provide more information regarding the microstructural evolution.

Again, the high-momentum part of the OEMS arose from positron annihilations with core electrons and hence contains information on the chemical identity of the atoms close to the positron annihilation site. The parameters *S* and *W* are commonly used to assess the chemical signatures of the annihilation sites and to estimate the relative positron annihilation with valence and core electrons, respectively. The low-momentum shape parameter *S* is the fraction of the low momentum annihilation defined by the specific P_L values in the momentum window from 0 to 0.4 a.u.. Since C and Si core electrons coexist in 3C-SiC, W_C and W_{Si} are the corresponding high momentum annihilation fractions, which are defined here as 1.1~1.7 a.u. and 2.2~3.2 a.u., respectively. Fig. 7 plots the S-W_C and S-W_{Si} pairs obtained from the OEMS data. Each data point in an S-W plot refers

to one specific microstructure. In irradiated pure metals, the (S, W) points generally fall on a line segment because only interstitial- and vacancy-type defect clusters are formed. Fig. 7 (a) shows an approximately linear relationship between S and W_C, which indicates that the Si vacancy-related defect responsible for positron trapping is the same under all of the irradiation conditions present in this study. This is consistent with the identified vacancy defects from PALS analysis, as shown in Fig. 7 (a).

In contrast, the correlation between S and W_{Si} (Fig. 7 (b)) was more complicated. This plot can be divided into two separate line segments. The first segment consisted of the samples irradiated to 0.01 dpa. Since the majority of the positrons were trapped in vacancy-type defects, W_{Si} arose from the positron annihilation with the core electrons of Si atoms around the positron trapping sites. Therefore, C-vacancy was contained in the detected vacancy type defect, which is consistent with the identification of $V_{Si} + V_C$ neutral clusters by positron lifetime analysis.

If the composition of the atoms surrounding the positron trapping sites in other samples has no change in comparison with that of the 3C-SiC irradiated to 0.01 dpa (i.e., those located on the first segment), the W_{Si} is expected to continuously decrease and fall on the extended parts (shown as a black dashed line in Fig. 7(b)) of the first segment with increasing radiation dose. However, the S-W_{Si} pairs of all other samples irradiated to > 0.1 dpa fall on a different line segment and W_{Si} has relatively larger values compared with the expected values based on the hypothesis that the chemical identity of the atoms surrounding the positron trapping sites is independent of the irradiation temperature and dose. This suggests that more Si atoms are surrounding the positron trapping sites and a new type of defect appears as the radiation dose increases. It could be an antisite defect, Si_C or C_{Si}, formed through the short range migration of Si and C, resulting in recombination with V_C and V_{Si} created during neutron irradiation. Considering that the formation energy of C_{Si} (1.32 eV) is much less than that of Si_C (7.20 eV) [32], it is expected that C_{Si} will be the prevalent type of anti-site. Moreover, the transformation of Si vacancy to V_C-C_{Si} complex becomes more and more significant with increasing temperature, resulting in an increase in the probability of positrons annihilating with core electrons of Si atoms. Therefore, the deduction that more C_{Si} is being generated is consistent with the CDB measurement showing that more Si atoms are surrounding the positron trapping sites with increasing irradiation dose.

4. Conclusions

Both PALS and CDB were used to investigate the vacancy defects in the neutron-irradiated 3C-SiC. The irradiation temperature and dose dependence of vacancy defects in SiC were captured by analyzing the measured positron lifetime spectra. The lifetime measurements indicated a minimal effect of irradiation temperature on vacancy defect evolution, presumably owing to the low thermal mobility of Si and C vacancies (they are essentially immobile) in the temperature regime of 380~540°C. Vacancy clusters were detected at higher radiation doses, as a result of either irradiation enhanced diffusion or displacement cascade overlap. For neutron irradiation temperatures above 750°C, an obvious increase in the long lifetime component of the positron lifetime was observed,

presumably owing to the mobility of Si vacancies leading to the formation of larger, stoichiometric V_{Si}+V_C clusters. These positron measurements and analyses of the positron lifetime components exclude the possibility that large vacancy clusters are generated in these neutron-irradiated 3C-SiC specimens in the temperature range from 380 to 790°C. The largest vacancy cluster that could be identified is the stoichiometric defect, $(V_{Si} + V_C)_4$, in a sample irradiated to 29 dpa at 750°C, in which Si vacancies are believed to have limited thermal mobility. CDB measurements helped to elucidate the chemical identities of the atoms surrounding the positron trapping sites. The irradiation temperature and dose dependence of vacancy defects derived from the OEMS was consistent with those derived from PALS analysis. S-W_C plot indicated that the Si vacancy related defects dominate in all studied materials. The deduction of C_{Si} production is consistent with the measured S-W_{Si} plot.

Last but not least, the volumetric swelling of neutron-irradiated 3C-SiC from vacancy clusters was predicted by utilizing the number density of the identified vacancy defects determined from a positron trapping model. The comparison with experimental data showed that the PAS-detectable vacancy clusters made only a minor contribution to the observed transient swelling of neutron-irradiated 3C-SiC. The present work suggests that more work is needed to elucidate the underlying mechanisms controlling the swelling of SiC exposed to neutron irradiation.

Acknowledgements

The work presented in this paper was partially supported by Laboratory Directed R&D funds at ORNL. The research was also sponsored by the US Department of Energy Office of Fusion Energy Science under grant DE-AC05-00OR22725 with UT-Battelle LLC, and grant DOE-DE-SC0006661 with the University of Tennessee, Knoxville. A portion of this research used resources at the High Flux Isotope Reactor, a DOE Office of Science User Facility operated by ORNL.

References

[1] L. L. Snead, T. Nozawa, Y. Katoh, T.-S. Byun, S. Kondo, and D. A. Petti, Journal of Nuclear Materials **371**, 329 (2007).
[2] R. J. Price, Nuclear Technology **35**, 320 (1977).
[3] Y. Katoh, L. L. Snead, I. Szlufarska, and W. J. Weber, Current Opinion in Solid State and Materials Science **16**, 143 (2012).
[4] A. Hasegawa, A. Kohyama, R. H. Jones, L. L. Snead, B. Riccardi, and P. Fenici, Journal of Nuclear Materials **283-287**, 128 (2000).
[5] S. J. Zinkle, K. A. Terrani, J. C. Gehin, L. J. Ott, and L. L. Snead, Journal of Nuclear Materials **448**, 374 (2014).
[6] R. J. Price, Journal of Nuclear Materials **48**, 47 (1973).
[7] V. A. Nikolaenko, V. G. Gordeyev, and V. N. Kuznetsov, Radiation Effects **27**, 163 (1976).
[8] Y. Katoh, N. Hashimoto, S. Kondo, L. L. Snead, and A. Kohyama, Journal of Nuclear Materials **351**, 228 (2006).

[9] L. L. Snead, Y. Katoh, T. Koyanagi, K. Terrani, and E. D. Specht, Journal of Nuclear Materials **471**, 92 (2016).
[10] T. Umeda, N. T. Son, J. Isoya, E. Janzen, T. Ohshima, N. Morishita, H. Itoh, A. Gali, and M. Bockstedte, Phys Rev Lett **96**, 145501 (2006).
[11] S. B. Orlinski, J. Schmidt, E. N. Mokhov, and P. G. Baranov, Physical Review B **67,** 125207 (2003).
[12] P. G. Baranov, I. V. Ilyin, A. A. Soltamova, and E. N. Mokhov, Physical Review B **77,** 085120 (2008).
[13] H. Itoh, M. Yoshikawa, I. Nashiyama, H. Okumura, S. Misawa, and S. Yoshida, Journal of Applied Physics **77**, 837 (1995).
[14] G. Alfieri and T. Kimoto, Applied Physics Letters **93**, 032108 (2008).
[15] C. T. Brigden, I. Farnan, and P. R. Hania, Journal of Nuclear Materials **444**, 92 (2014).
[16] F. Tuomisto and I. Makkonen, Reviews of Modern Physics **85**, 1583 (2013).
[17] C. C. Ling, A. H. Deng, S. Fung, and C. D. Beling, Applied physics A **70**, 33 (2000).
[18] R. Aavikko, K. Saarinen, F. Tuomisto, B. Magnusson, N. T. Son, and E. Janzén, Physical Review B **75,** 085208 (2007).
[19] A. Kawasuso, H. Itoh, S. Okada, and H. Okumura, Journal of Applied Physics **80**, 5639 (1996).
[20] M. Akiyoshi, H. Tsuchida, I. Takagi, T. Yoshiie, X. Qiu, K. Sato, and T. Yano, Journal of Nuclear Science and Technology **49**, 595 (2012).
[21] G. Brauer, W. Anwand, and e. al., Physical Review B **54**, 3084 (1996).
[22] G. Brauer, M. S. Anand, and e. al., Physical Review B **54**, 2512 (1996).
[23] S. Dannefaer, D. Craigen, and D. Kerr, Physical Review B **51**, 1928 (1995).
[24] L. Henry, M. F. Barthe, C. Corbel, P. Desgardin, G. Blondiaux, S. Arpiainen, and L. Liszkay, Physical Review B **67,** 115210 (2003).
[25] A. Kawasuso, H. Itoh, D. B. Cha, and S. Okada, Materials Science Forum **264-268**, 611 (1998).
[26] A. Kawasuso, H. Itoh, N. Morishita, M. Yoshikawa, T. Ohshima, I. Nashiyama, S. Okada, H. Okumura, and S. Yoshida, Applied physics A **67**, 209 (1998).
[27] Q. Xu, T. Yoshiie, and M. Okada, Journal of Nuclear Materials **386-388**, 169 (2009).
[28] Y. Katoh, L. L. Snead, C. M. Parish, and T. Hinoki, Journal of Nuclear Materials **434**, 141 (2013).
[29] X. Hu, T. Koyanagi, M. Fukuda, Y. Katoh, L. L. Snead, and B. D. Wirth, Journal of Nuclear Materials **470**, 278 (2016).
[30] P. Kirkegaard, J. V. Olsen, and M. Eldrup, http://palsfit.dk (2016).
[31] M. Bockstedte, A. Mattausch, and O. Pankratov, Physical Review B **68,** 205201 (2003).
[32] F. Gao, E. J. Bylaska, W. J. Weber, and L. R. Corrales, Physical Review B **64**, 245208 (2001).
[33] L. Torpo, M. Marlo, T. Staab, and R. M. Nieminen, J. Phys.: Condens. Matter **13**, 6203 (2001).
[34] N. T. Son, B. Magnusson, Z. Zolnai, A. Ellison, and E. Janzén, Materials Science Forum **433-436**, 45 (2003).

[35] J. Wiktor, X. Kerbiriou, G. Jomard, S. Esnouf, M.-F. Barthe, and M. Bertolus, Physical Review B **89,** 155203 (2014).
[36] J. Wiktor, G. Jomard, M. Torrent, and M. Bertolus, Physical Review B **87,** 235207 (2013).
[37] M. Bockstedte, A. Gali, T. Umeda, N. T. Son, J. Isoya, and E. Janzén, Materials Science Forum **527-529**, 539 (2006).
[38] M. Bockstedte, A. Gali, A. Mattausch, O. Pankratov, and J. W. Steeds, physica status solidi (b) **245**, 1281 (2008).
[39] H. Ceeh, C. Hugenschmidt, K. Schreckenbach, S. A. Gärtner, P. G. Thirolf, F. Fleischer, and D. Schwalm, Physical Review A **84,** 062508 (2011).
[40] F. Gao and W. J. Weber, Physical Review B **63,** 054101 (2000).
[41] R. W. Siegel, Ann. Rev. Mater. Sci. **10**, 393 (1980).
[42] Y. Katoh, K. Ozawa, C. Shih, T. Nozawa, R. J. Shinavski, A. Hasegawa, and L. L. Snead, Journal of Nuclear Materials **448**, 448 (2014).
[43] J. M. Campillo Robles, E. Ogando, and F. Plazaola, J Phys Condens Matter **19**, 176222 (2007).

Table Captions

Table 1. Irradiation conditions of 3C-SiC in HFIR.

Table 2. The fitted long positron lifetimes (τ_2) of neutron-irradiated 3C-SiC and possible vacancy clusters that have positron lifetimes comparable to those of the measured values.

Table 3 The positron trapping rates, the corresponding specific trapping coefficients, and the resulting calculated concentrations of the vacancy defects in neutron-irradiated 3C-SiC.

Figure Captions

Fig. 1 Comparison of normalized positron lifetime spectra of neutron-irradiated 3C-SiC at temperatures of (a) 380~440°C, (b) 500~540°C, and (c) 750~790°C at various dose levels. The lifetime spectrum of the as-received 3C-SiC is shown in the black symbols for comparison.

Fig. 2 Comparison of normalized positron lifetime spectra of neutron irradiated 3C-SiC at a dose of (a) 0.1 dpa and (b) ~30 dpa, respectively, at various irradiation temperature.

Fig. 3 Short (τ_1) and long (τ_2) positron lifetime and the associated intensity of τ_2 resulting from analysis of the measured positron lifetime spectra of neutron-irradiated 3C-SiC as a function of dose at various irradiation temperatures. The analysis results for as-received 3C-SiC are also shown for comparison. The identification of the possible vacancy defect clusters is also shown in the figure of the long lifetime (τ_2). The black hollow symbols shown in the bottom figure correspond to calculated lifetime values for τ_1 obtained from the trapping model assuming the presence of one type of defect only.

Fig. 4 Comparison of volume swelling derived from PAS lifetime analysis and measured swelling as a function of radiation dose.

Fig. 5. The ratio curves of the normalized OEMS of neutron-irradiated 3C-SiC to that of unirradiated 3C-SiC. (a) 380~440°C, (b) 500~540°C, and (c) 750~790°C

Fig. 6 OEMS ratio to UHP Si and C to determine the relative position of C and Si peaks

Fig. 7 (a) S-W_C and (b) S-W_{Si} plots for neutron irradiated 3C-SiC. The identified vacancy defects from PALS analysis were also shown in (a).

Table 1. Irradiation conditions of 3C-SiC in HFIR

Sample ID	Irradiation temperature (°C)	Irradiation dose (dpa)
T8A1	380	0.01
T8A2	380	0.11
TTN01	380	1.5
TTN03	440	31
T8B1	540	0.01
T8B2	540	0.11
TTN05	500	29
T8D1	790	0.11
T8E1	760	1.4
TTN07	750	29

Table 2. The fitted long positron lifetimes (τ_2) of neutron-irradiated 3C-SiC and possible vacancy clusters that have positron lifetimes comparable to those of the measured values

Samples	Fitted long lifetime, τ_2, (ps)	Defect	Theoretical positron lifetime* (ps)
As-received	196	V_{Si}^-	185~210[21]
T8A1	239	$V_{Si} + V_C$	235, 242[35]
T8A2	255	$2V_C + V_{Si}$	243, 250[35]
TTN01	256	$2V_C + V_{Si}$	243, 250[35]
TTN03	263	$(V_{Si} + V_C)_2$	262, 269[35]
T8B1	247	$V_{Si} + V_C$	235, 242[35]
T8B2	252	$2V_C + V_{Si}$	243, 250[35]
TTN05	275	$(3V_{Si} + 2V_C)^-$	-
T8D1	266	$(V_{Si} + V_C)_2$	262, 269[35]
T8E1	287	$(V_{Si} + V_C)_3$	286[21]
TTN07	294	$(V_{Si} + V_C)_4$	-

* For the values obtained from Ref. [35], the first value is the calibrated lifetime based on a ratio, which was obtained by scaling the calculated positron lifetime (144 ps) of perfect 3C-SiC to the experimentally obtained value (140 ps).; the second value is directly obtained from simulations.

Table 3 The positron trapping rates, the corresponding specific trapping coefficients, and the resulting calculated concentrations of the vacancy defects in neutron-irradiated 3C-SiC.

Samples	Trapping rate, κ, ($\times 10^9$ s)	Specific trapping coefficient, μ, ($\times 10^{14}$ s^{-1})	Concentration (appm)
As-received	6.1	11.0	5.6
T8A1	30.8	6.3	49.0
T8A2	38.1	7.0	27.1
TTN01	48.1	7.0	34.3
TTN03	69.6	10.0	69.8
T8B1	63.4	6.3	101.0
T8B2	70.6	7.0	50.4
TTN05	61.9	25.1	24.7
T8D1	54.1	10.0	54.3
T8E1	42.1	13.1	32.2
TTN07	94.7	15.8	59.9

Fig. 1 Comparison of normalized positron lifetime spectra of neutron-irradiated 3C-SiC at temperatures of (a) 380~440°C, (b) 500~540°C, and (c) 750~790°C at various dose levels. The lifetime spectrum of the as-received 3C-SiC is shown in the black symbols for comparison.

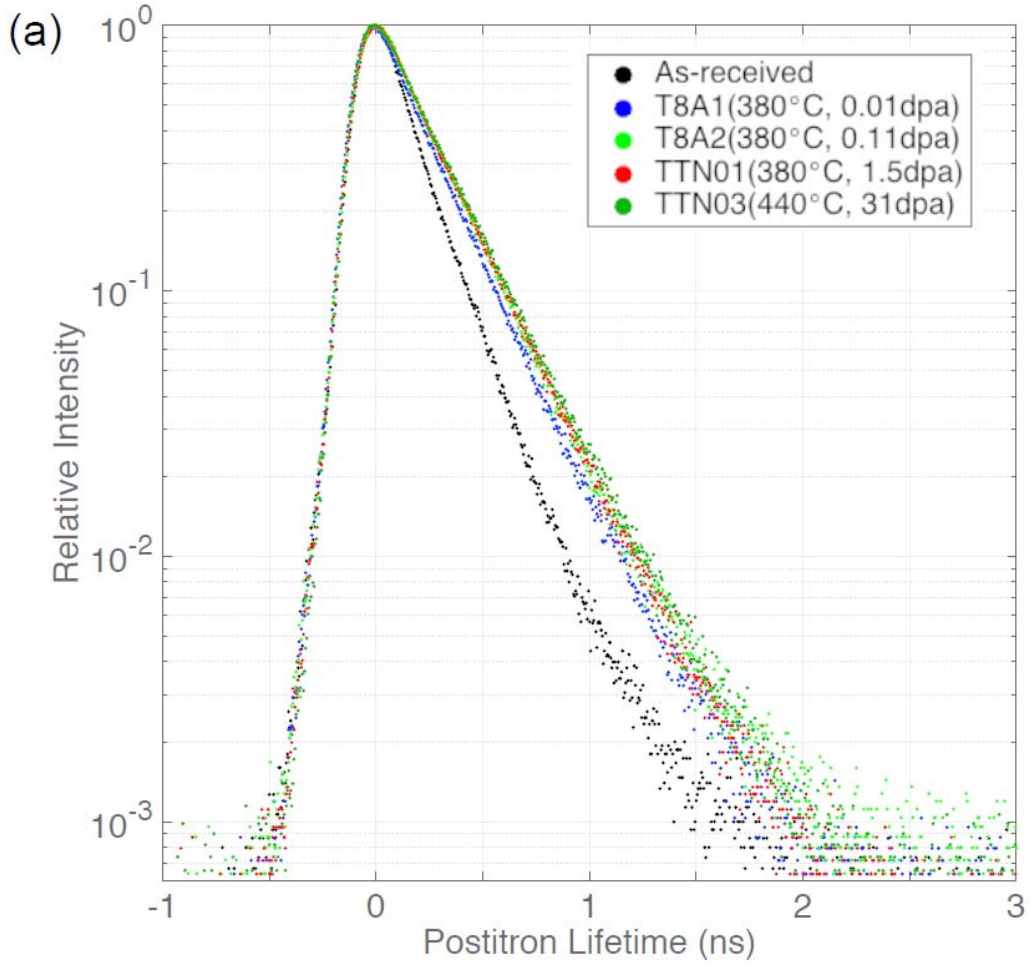

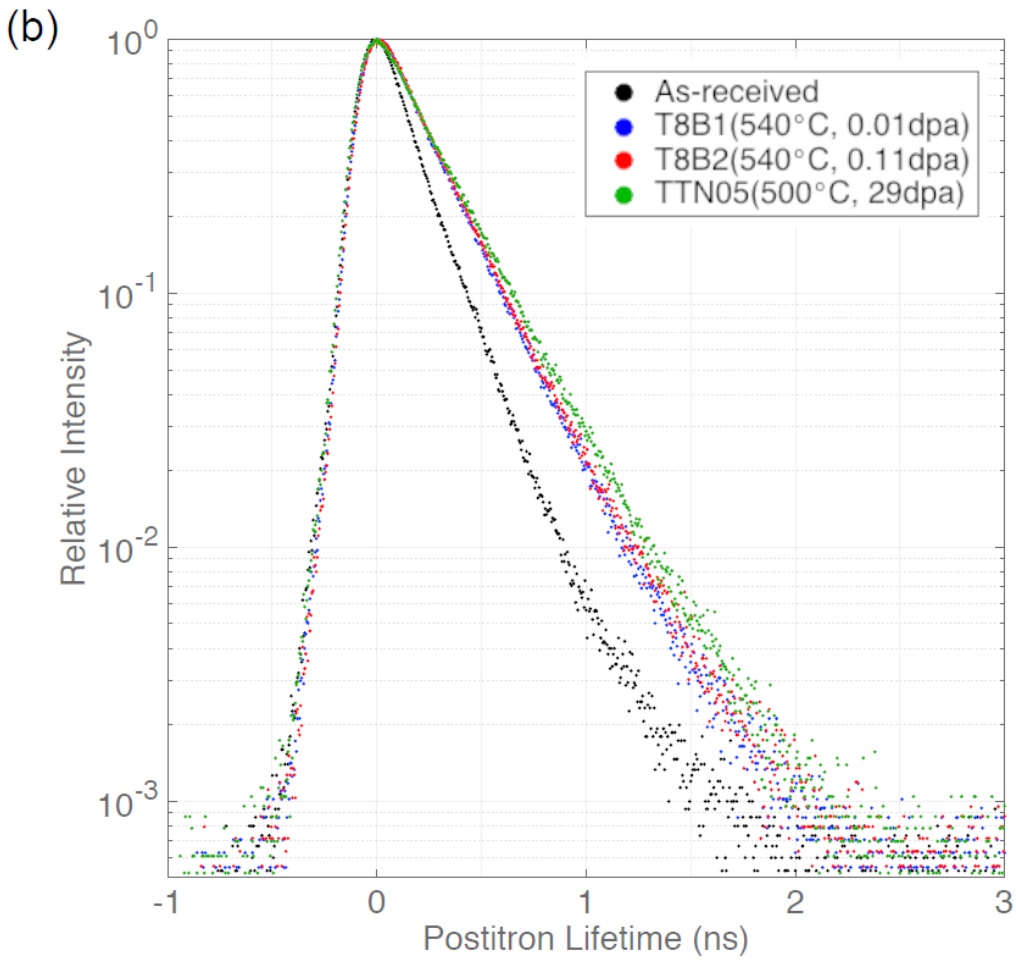
(b)
As-received
T8B1(540°C, 0.01dpa)
T8B2(540°C, 0.11dpa)
TTN05(500°C, 29dpa)
Relative Intensity
Postitron Lifetime (ns)

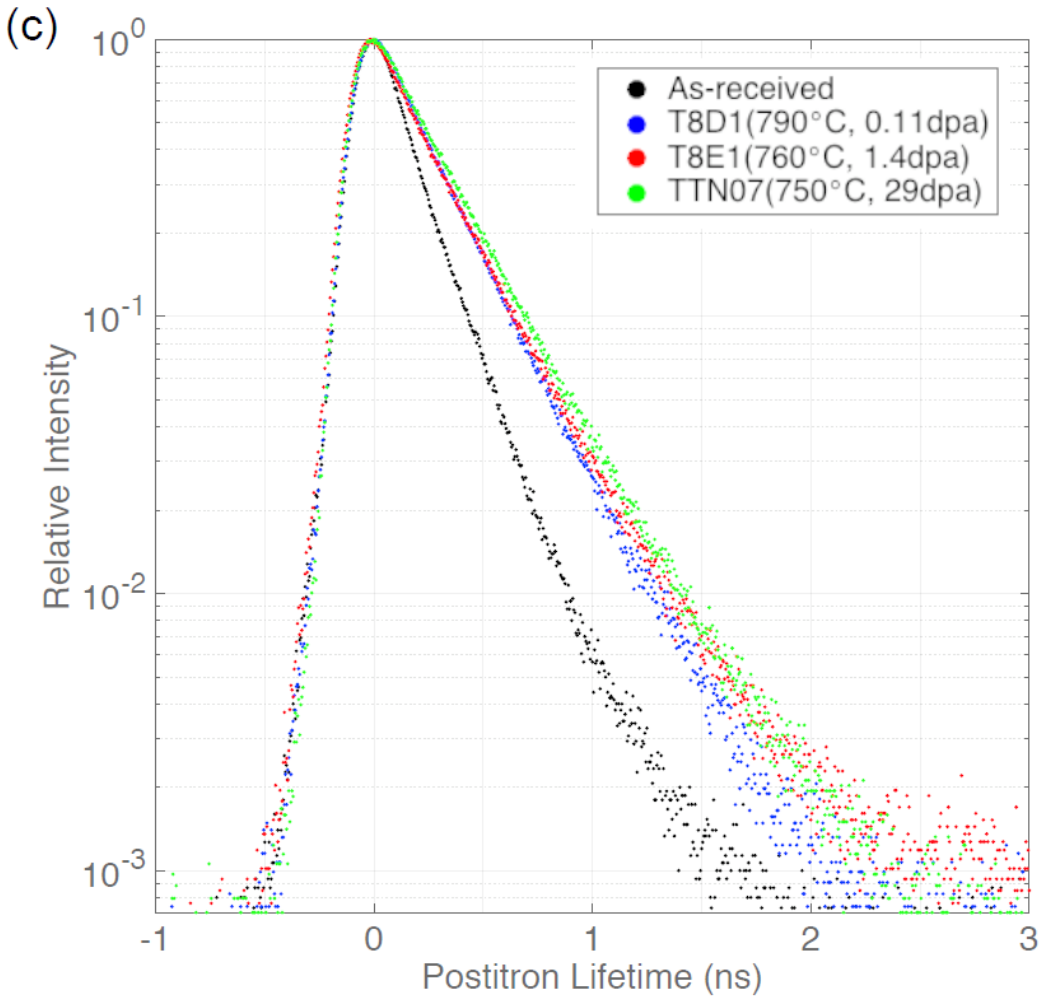
(c)
As-received
T8D1(790°C, 0.11dpa)
T8E1(760°C, 1.4dpa)
TTN07(750°C, 29dpa)
Relative Intensity
Postitron Lifetime (ns)

Fig. 2 Comparison of normalized positron lifetime spectra of neutron irradiated 3C-SiC at a dose of (a) 0.1 dpa and (b) ~30 dpa, respectively, at various irradiation temperature.

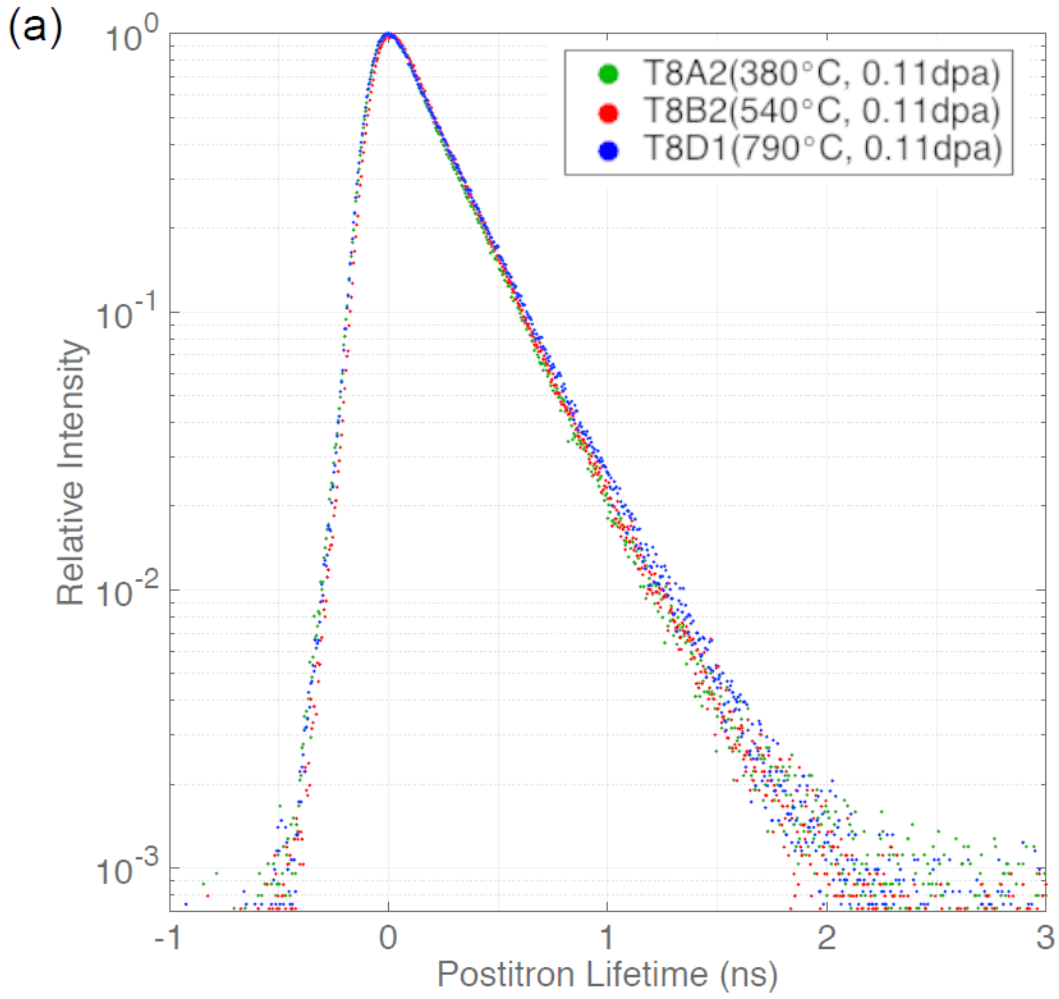

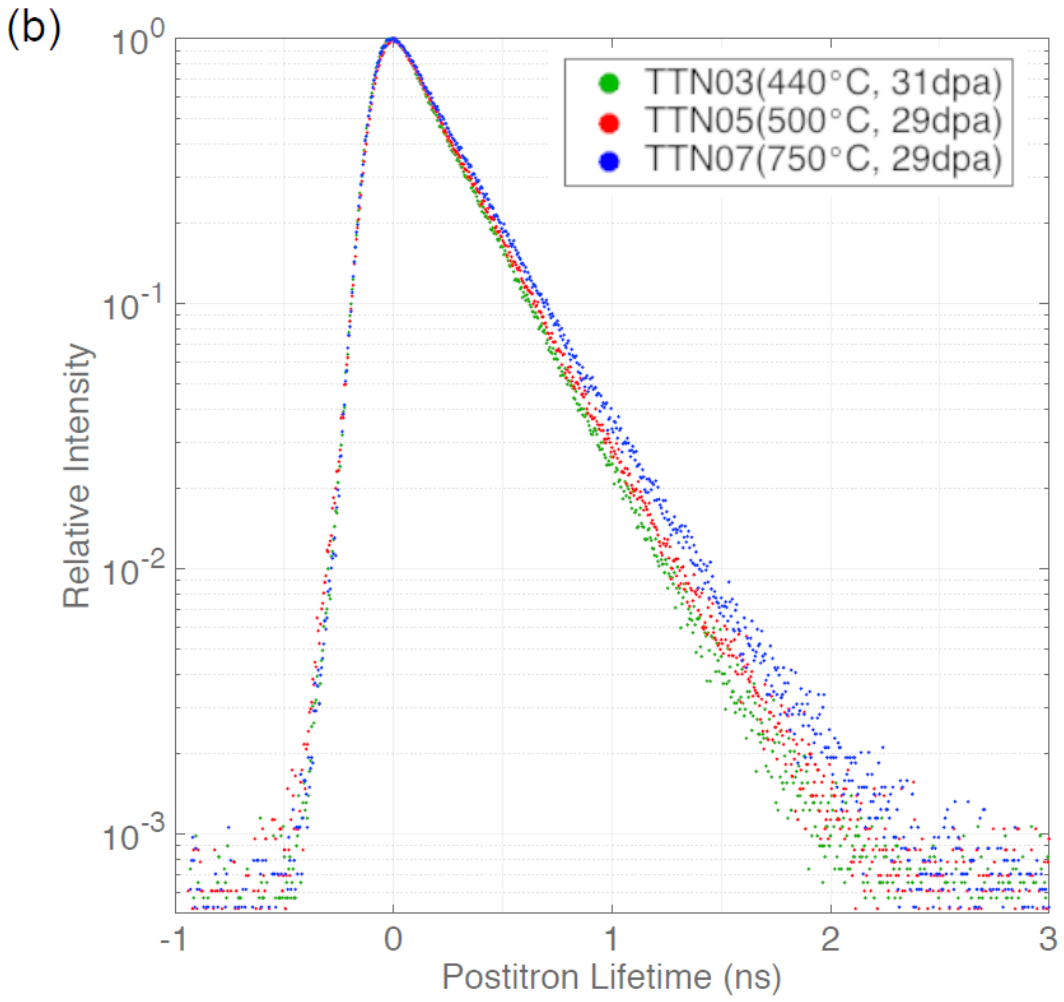
(b)
TTN03(440°C, 31dpa)
TTN05(500°C, 29dpa)
TTN07(750°C, 29dpa)
Relative Intensity
Postitron Lifetime (ns)

Fig. 3 Short (τ_1) and long (τ_2) positron lifetime and the associated intensity of τ_2 resulting from analysis of the measured positron lifetime spectra of neutron-irradiated 3C-SiC as a function of dose at various irradiation temperatures. The analysis results for as-received 3C-SiC are also shown for comparison. The identification of the possible vacancy defect clusters is also shown in the figure of the long lifetime (τ_2). The black hollow symbols shown in the bottom figure correspond to calculated lifetime values for τ_1 obtained from the trapping model assuming the presence of one type of defect only.

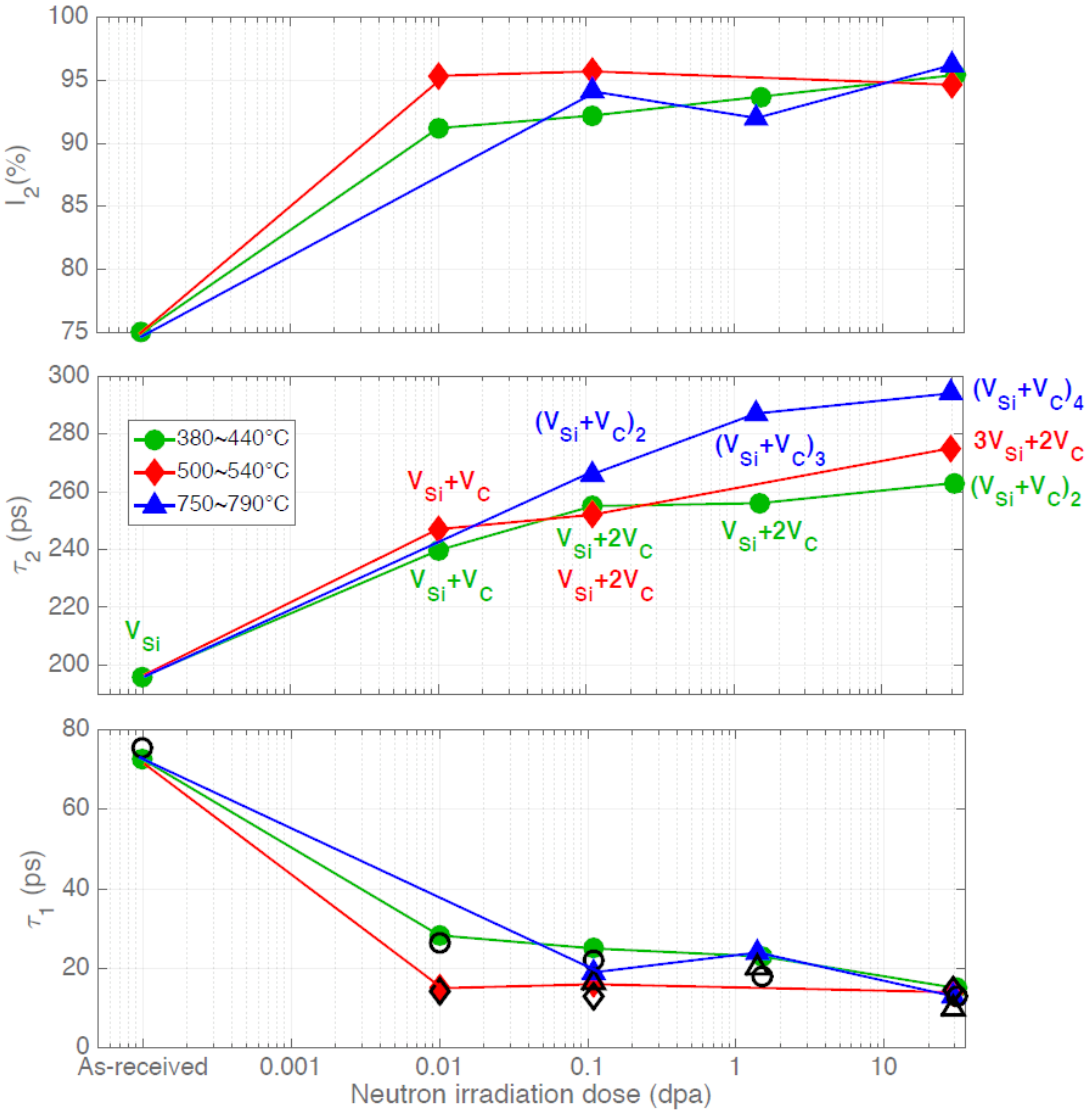

Fig. 4 Comparison of volume swelling derived from PAS lifetime analysis and measured swelling as a function of radiation dose.

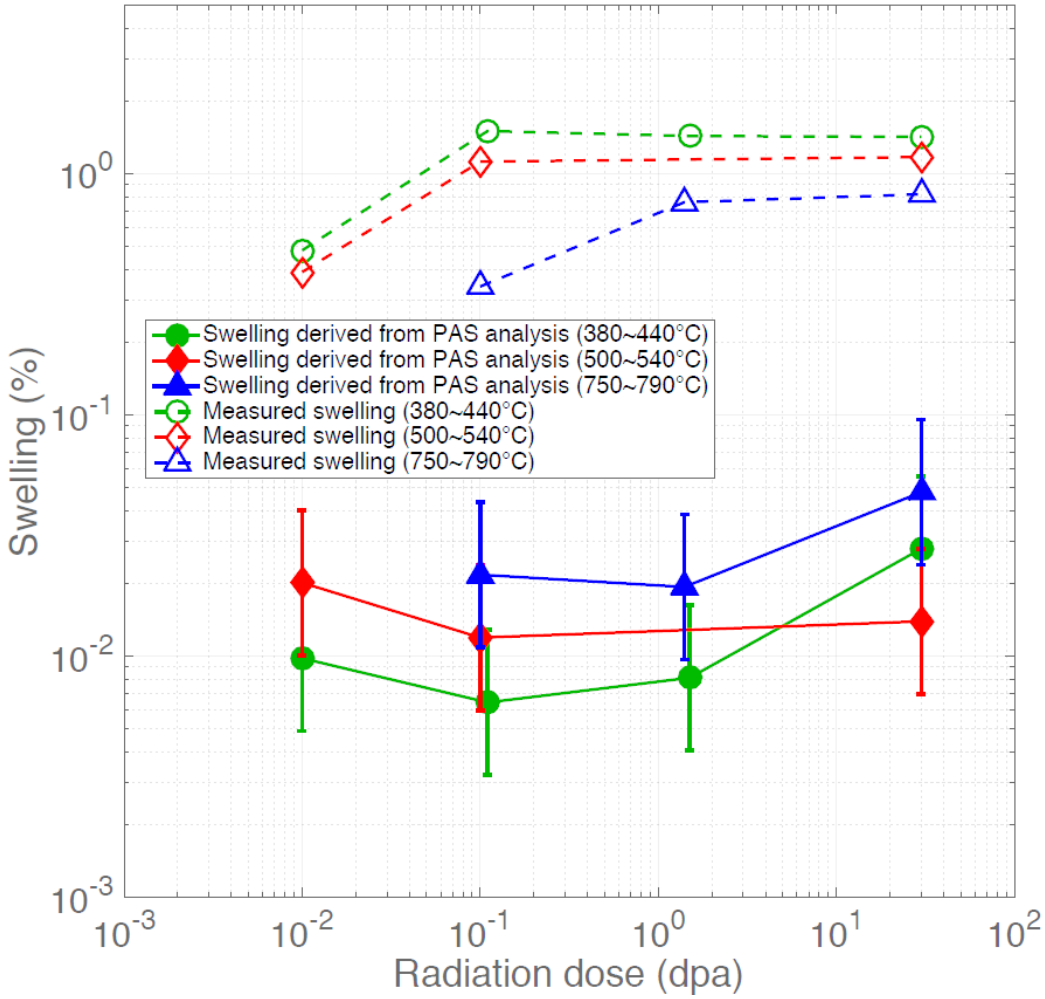

Fig. 5. The ratio curves of the normalized OEMS of neutron-irradiated 3C-SiC to that of unirradiated 3C-SiC. (a) 380~440°C, (b) 500~540°C, and (c) 750~790°C

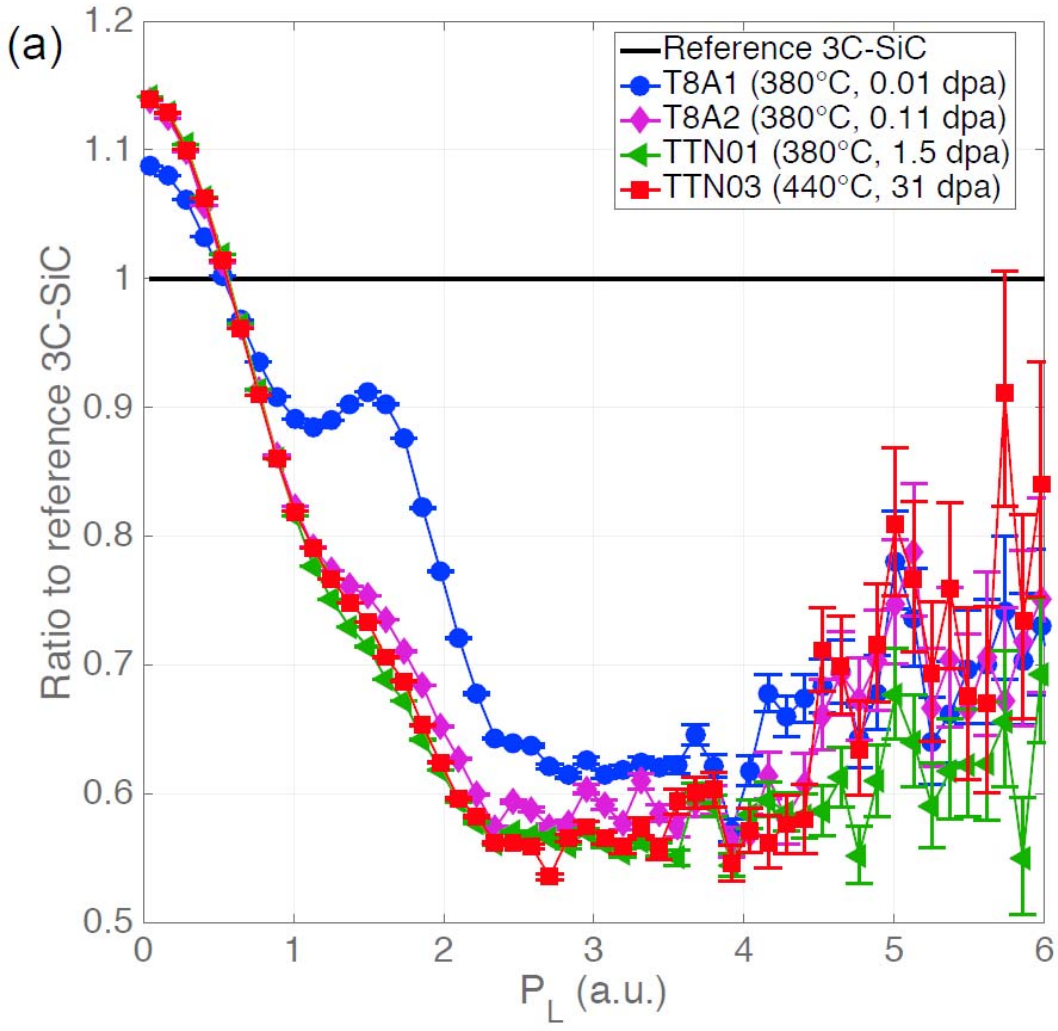

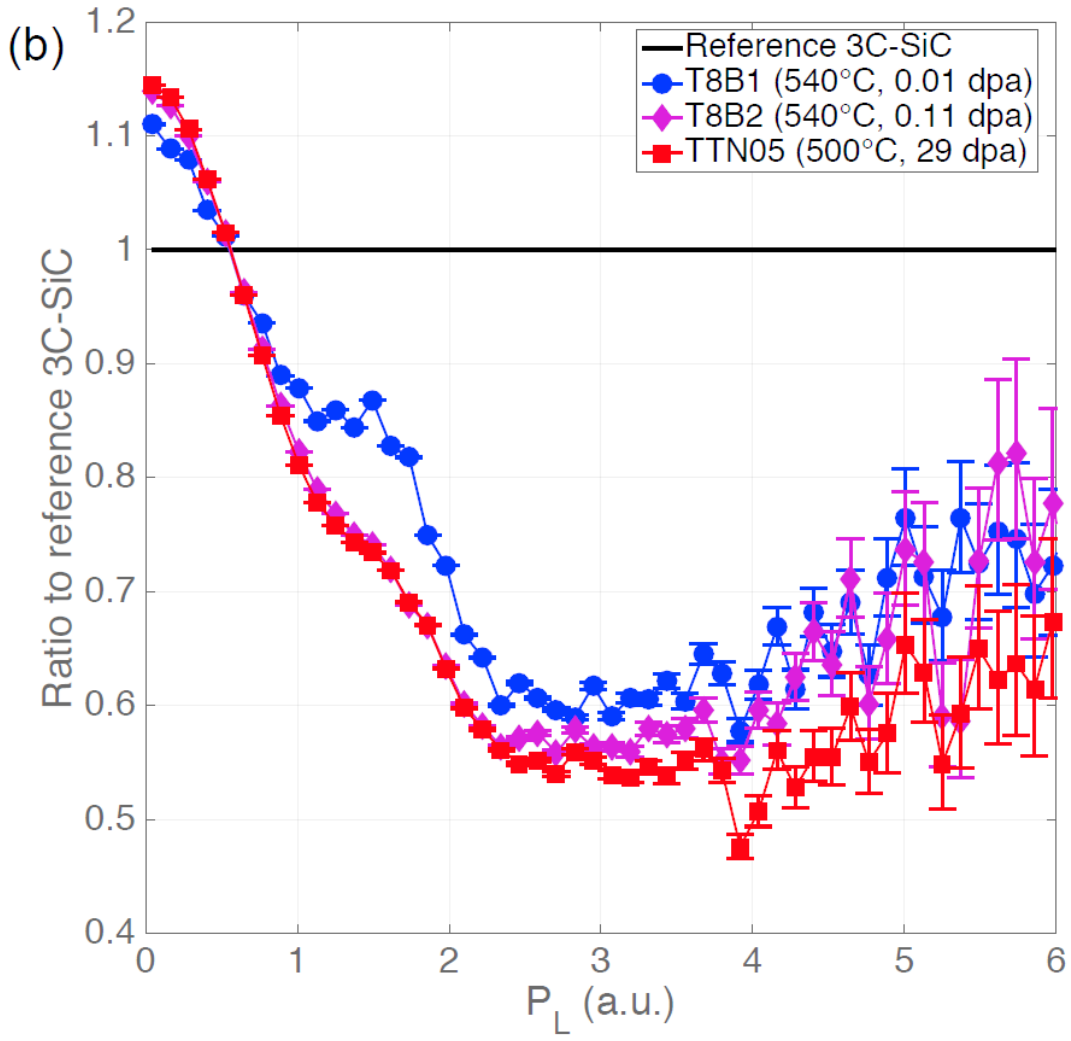
(b)
Reference 3C-SiC
T8B1 (540°C, 0.01 dpa)
T8B2 (540°C, 0.11 dpa)
TTN05 (500°C, 29 dpa)
Ratio to reference 3C-SiC
P_L (a.u.)
1.2
1.1
1
0.9
0.8
0.7
0.6
0.5
0.4
0
1
2
3
4
5
6

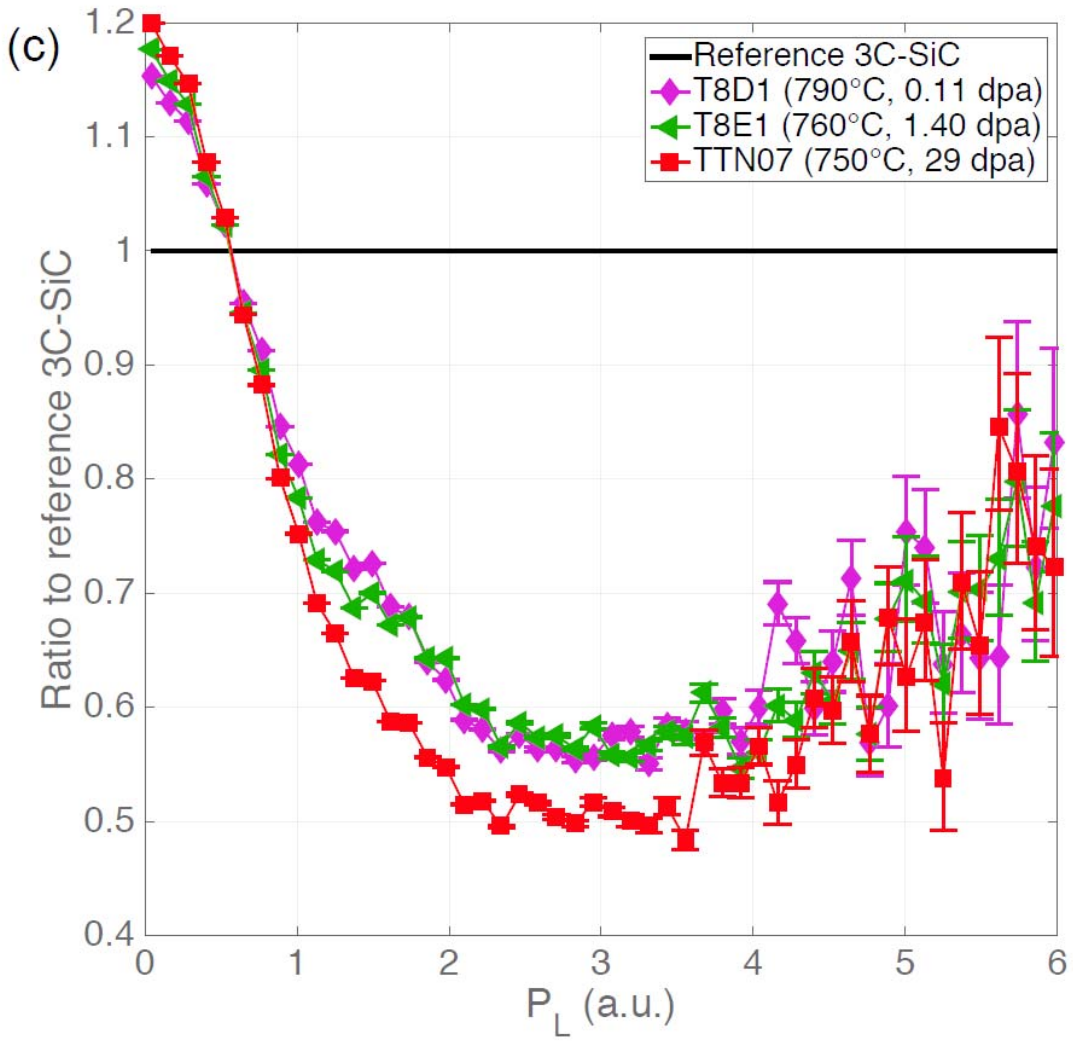
(c)
Reference 3C-SiC
T8D1 (790°C, 0.11 dpa)
T8E1 (760°C, 1.40 dpa)
TTN07 (750°C, 29 dpa)
Ratio to reference 3C-SiC
P_L (a.u.)
1.2
1.1
1
0.9
0.8
0.7
0.6
0.5
0.4
0
1
2
3
4
5
6

Fig. 6 OEMS ratio to UHP Si and C to determine the relative position of C and Si peaks

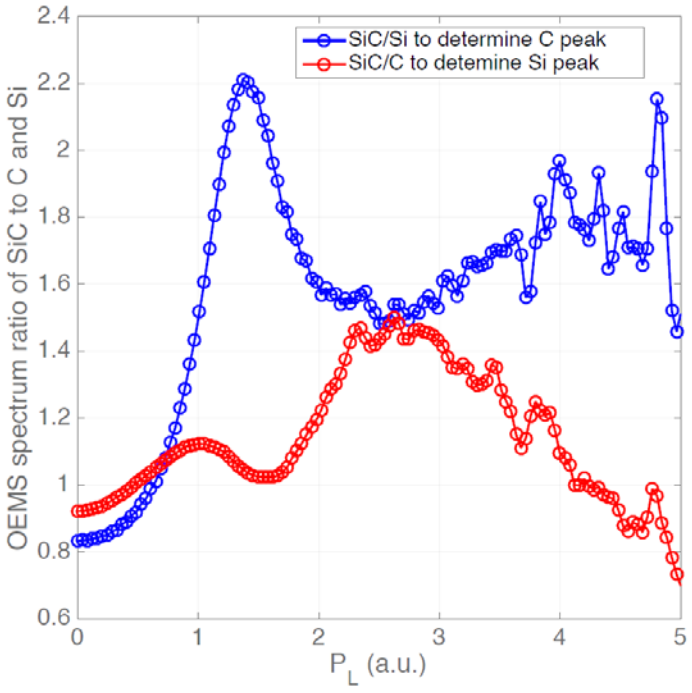

Fig. 7 (a) S-W_C and (b) S-W_{Si} plots for neutron irradiated 3C-SiC. The identified vacancy defects from PALS analysis were also shown in (a).

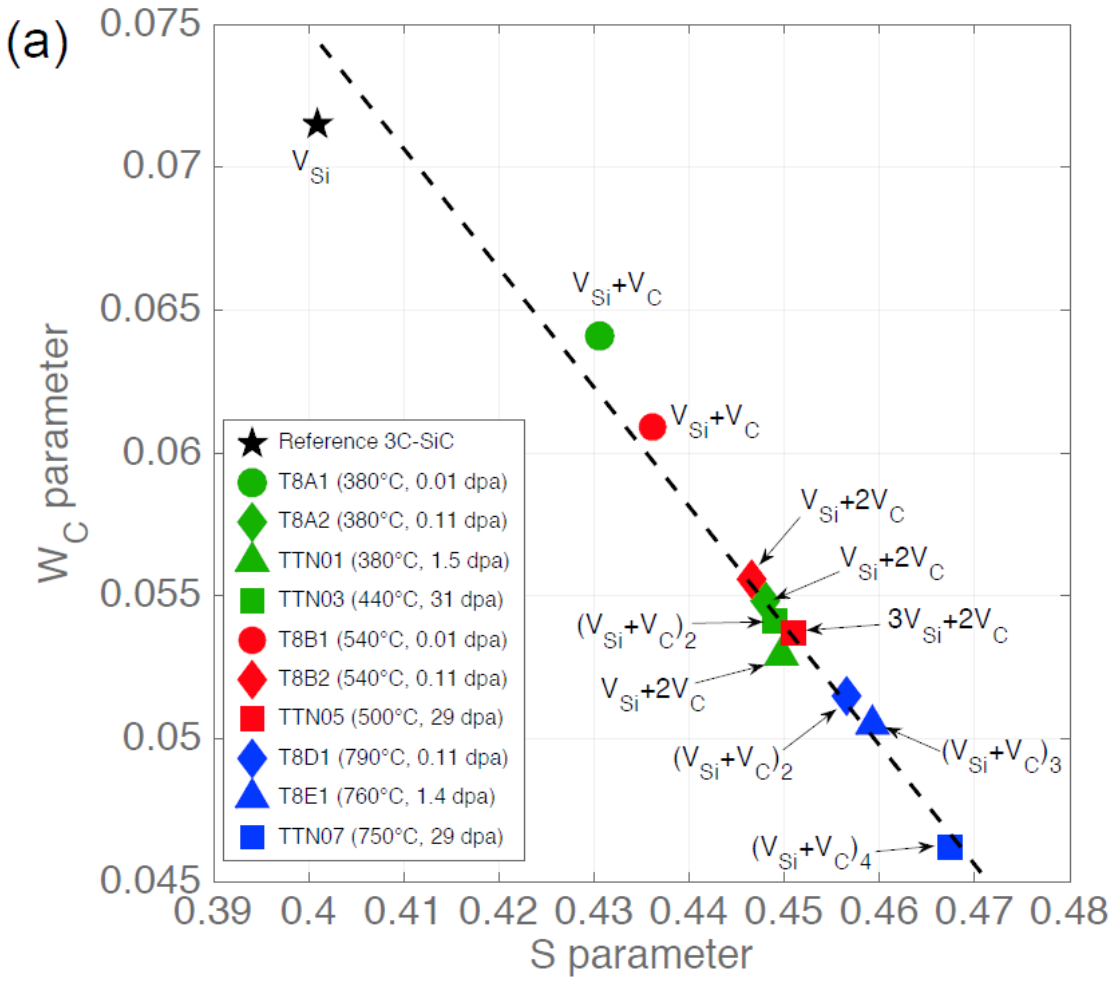

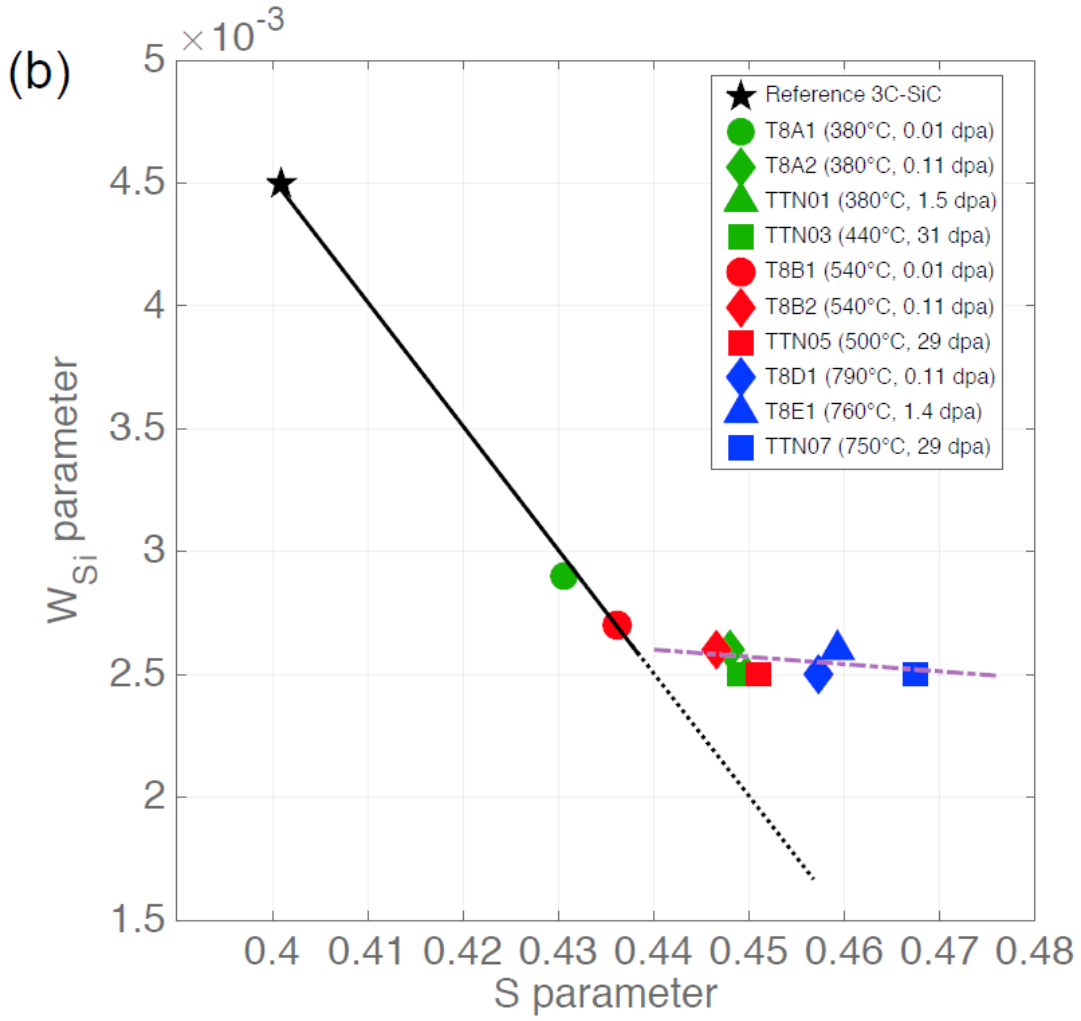
(b)
×10-3
5
4.5
4
3.5
3
2.5
2
1.5
W_Si parameter
0.4
0.41
0.42
0.43
0.44
0.45
0.46
0.47
0.48
S parameter
Reference 3C-SiC
T8A1 (380°C, 0.01 dpa)
T8A2 (380°C, 0.11 dpa)
TTN01 (380°C, 1.5 dpa)
TTN03 (440°C, 31 dpa)
T8B1 (540°C, 0.01 dpa)
T8B2 (540°C, 0.11 dpa)
TTN05 (500°C, 29 dpa)
T8D1 (790°C, 0.11 dpa)
T8E1 (760°C, 1.4 dpa)
TTN07 (750°C, 29 dpa)